OPTICAL MODELING OF THE INTERNAL BACK REFLECTANCE OF VARIOUS C-SI DIELECTRIC STACKS FEATURING ALO_x, SIN_X, TIO_2 AND SIO_2

K.O. Davis[1,2], H.P. Seigneur[1], K. Jiang[3], C. Demberger[3], H. Zunft[3], H. Haverkamp[3], D. Habermann[3], and W.V. Schoenfeld[1,2]
[1]Florida Solar Energy Center, University of Central Florida, Cocoa, FL, U.S.
[2]CREOL, College of Optics and Photonics, University of Central Florida, Orlando, FL, U.S.
[3]Gebr. Schmid GmbH & Co., Robert-Bosch-Str. 32 - 34, 72250 Freudenstadt, Germany

ABSTRACT

One promising path to a reduced cost of crystalline silicon (c-Si) photovoltaics (PV) is to increase silicon usage efficiency by using thinner wafers. Many challenges arise when transitioning to thin wafer cells, including increased surface recombination at the rear side of the cell, increased wafer bowing, and a reduction in optical absorption due to a decreased optical path length within the silicon. Rear side passivation provides great promise in addressing these challenges. This paper addresses rear side dielectric configurations that can optimize back surface reflectance, in addition to providing excellent surface passivation. Optical modeling of various stack configurations is examined to explore the back surface reflectance at the Si-dielectric interface for different film combinations and thicknesses as a function of wavelength and internal angle of incidence. Specifically, configurations using aluminum oxide (AlO_x), silicon nitride (SiN_x), titanium dioxide (TiO_2), and silicon dioxide (SiO_2) were investigated with a focus on designing stack configurations that will also allow for high quality passivation and are compatible with a high-volume manufacturing environment.

INTRODUCTION

A large portion of the cost of a final c-Si PV module is due to the silicon used to create the solar cells [1]. Thin wafers (e.g. < 150 µm) have received much attention due to the potential to significantly reduce module cost [2-4]. There are still many challenges associated with processing thin silicon wafers including: wafer handling [5]; wafer bowing when using a full Al back contact [6]; surface recombination at the back side of the cell [7]; and reduced absorption of near-bandgap photons [8].

In-line deposition of rear side dielectric passivation layers has emerged as a strong candidate to realize PERC-type solar cells, which address the issues of wafer bowing and rear side surface recombination. This paper focuses on modeling the optical properties of various single and double layer dielectric stack configurations, with particular attention to the backside internal reflectance at the Si-dielectric interface.

In particular, various layer combinations and thicknesses are investigated with the intent to optimize the internal back reflectance (BR) for near bandgap photons. Higher reflectance effectively increases the optical path length of the cell, which can lead to increased absorption, particularly at longer wavelengths, which are poorly absorbed in c-Si due to the indirect bandgap. This is highlighted in Fig. 1 where the fraction of light absorbed in c-Si as a function of wafer thickness is given for five wavelengths between 750 nm - 1050 nm using published extinction coefficients [9].

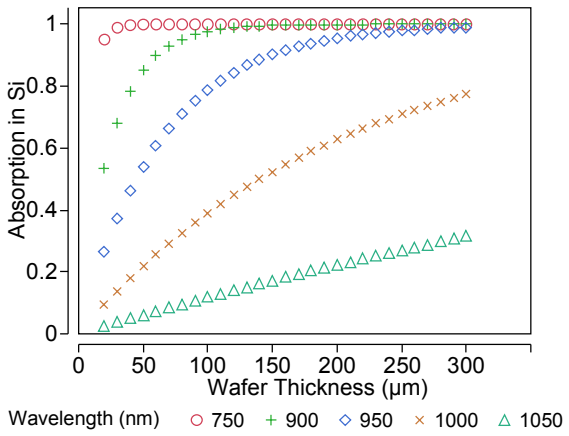

Figure 1: Optical absorption in c-Si as a function of wafer thickness for five different wavelengths between 750 nm - 1050 nm, calculated using published extinction coefficient data for Si [9].

AlO_x has gained significant attention as a rear side passivation material for p-type solar cells. Surface recombination velocities below 13 cm/s have been achieved with this material, and it possesses many advantages over other materials [10]. In an industrial PERC cell design, the thin AlO_x film will likely require a capping layer to prevent the screen printed Al paste from penetrating through the AlO_x, and the capping layer should add little cost. Therefore, dielectric stack configurations using AlO_x have recently been explored experimentally, including AlO_x-SiN_x and AlO_x-SiO_2 [11,12]. The dielectric stack configurations considered in this simulation study all consist of an AlO_x passivation layer of at least 10 nm thick to ensure compatibility with well designed p-type PERC cells, in terms of effective chemical and field effect passivation (Fig. 2). A single AlO_x layer is used as a reference case. Additionally, stacks featuring SiN_x, TiO_2 and SiO_2 capping layers are investigated.

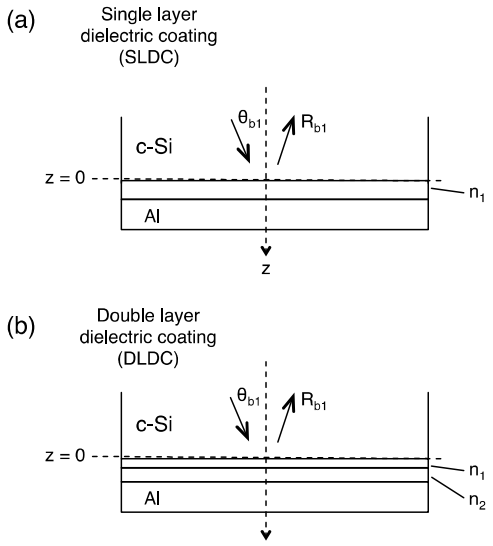

Figure 2: Dielectric stack configurations simulated in this study: (a) single layer dielectric coating and (b) double layer dielectric coating (AlO_x-TiO_2, AlO_x-SiO_2, AlO_x-SiN_x).

METHODOLOGY

Much of the previous work related to characterizing the internal BR of c-Si solar cells has relied on the utilization of experimentally measured internal quantum efficiency (IQE) and calculating the aggregate BR over all relevant wavelengths using raytracing software and solar cell simulation tools, such as RAYN and SUNRAYS [13]. In addition, much of this work has focused on SiO_2 and SiN_x film stacks.

This simulation study has been carried out by first directly simulating the internal BR, irrespective of the cell electronic properties, similar to the treatment by Green [14], but expanded to include multiple materials and stack configurations and different frontside optics (e.g. with and without encapsulation). Here the relative internal BR is calculated for various wavelengths (λ), angles of incidence between the silicon and initial dielectric layer (θ_{b1}) and various dielectric configurations (both in terms of material combinations and thicknesses). The goal is to provide new insight and a starting point for comparing the various dielectric configurations.

The transfer matrix method [15] of calculating multilayer transmission/reflectance using optical admittances of each medium is used to determine internal BR as a function of layer thickness for the different stack configurations at four near-bandgap wavelengths (900 nm, 950 nm, 1000 nm, 1050 nm) and as a function of θ_{b1}. In this treatment, the dielectric layers are assumed to be lossless (k = 0), and the assumed values are given in Table 1, taken from both the literature [9,16] and our spectroscopic ellipsometry measurements carried out on films deposited by atmospheric pressure chemical vapor deposition (APCVD) and plasma-enhanced CVD. For the Si and Al layers, the complex refractive index parameters are used throughout the calculations to account for losses due to the evanescent wave occurring for angles beyond the critical angle (θ_c). This last point is crucial, since the critical angle between Si and AlO_x is ≈26.5° (n_{AlOx} = 1.6, λ = 1000 nm), and the angle of incidence of most of the radiation on the backside is larger than this. This means the surface wave and evanescent losses are the dominant loss mechanisms for internal BR with these types of cell configurations.

Dielectric Layer	*Refractive Index*
AlO_x	1.60
SiO_2	1.46
TiO_2	2.00*
SiN_x (unencapsulated)	2.06
SiN_x (encapsulated)	2.20

Table 1: Assumed refractive index values for dielectrics
* It should be noted that the refractive index of TiO_2 changes significantly depending on process conditions.

For textured monocrystalline wafers, the characteristic base angle (α) of the well-known pyramid structures is commonly taken to be 54.74°, although recent work has shown that in industrial cells this is actually around 50-52° depending on the etchant used [17]. Assuming α = 54.74° and a SiO_2 frontside coating, Kray *et al.* show that at normal incidence, the two primary rays transmitted through the cell have an angle of incidence (AOI) on the backside of 41.4° and 59.1°, the former (Ray A) being the primary ray, which carries 76.4% of the total incident flux and the latter (Ray B) carrying 19.4% [13]. This is illustrated in Fig. 3. Using simple geometrical optics equations, one can show that the primary ray for a similar cell with a SiN_x anti-reflection coating (ARC) has an equivalent backside AOI. However, the backside AOI of the primary ray for an encapsulated cell is significantly lower at ≈35° (n_{EVA} = 1.5, n_{SiNx} = 2.2).

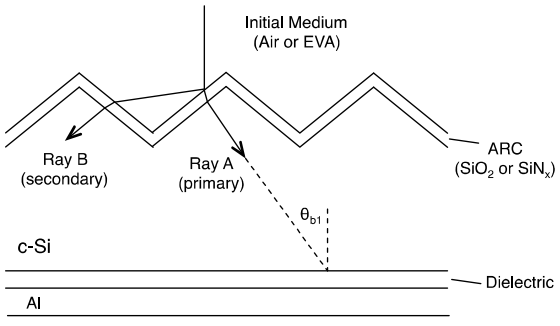

Figure 3: Schematic illustrating two primary transmitted rays in a textured monocrystalline solar cell (from Reference 13). Note: the backside AOI of the primary ray for an encapsulated cell is smaller (35°) than that of an unencapsulated cell (41.4°).

RESULTS AND DISCUSSION

By plotting contour maps of the internal BR vs. dielectric layer thickness and θ_{b1}, some interesting trends can be seen. For example, there are three critical regions in terms of the backside AOI, as shown in Fig. 4.

- Region I ($\theta_{b1} < \theta_c$): In this region, interference effects play a key role, hence the periodic dependence on layer thickness (constructive vs. destructive interference). These angles are less interesting for anisotropically etched monocrystalline cells, due to the light scattering of the primary beams, but could be of interest in cells with different texturing and ARC configurations (e.g. black silicon).
- Region II (θ_{b1} near θ_c): This region features significant losses due to the surface wave propagating along the Si-AlO_x interface, allowing for more energy transfer to the lossy Al layer.
- Region III ($\theta_{b1} > \theta_c$): Above the critical angle, a thicker dielectric layer means higher internal BR due to the further separation from the Al layer.

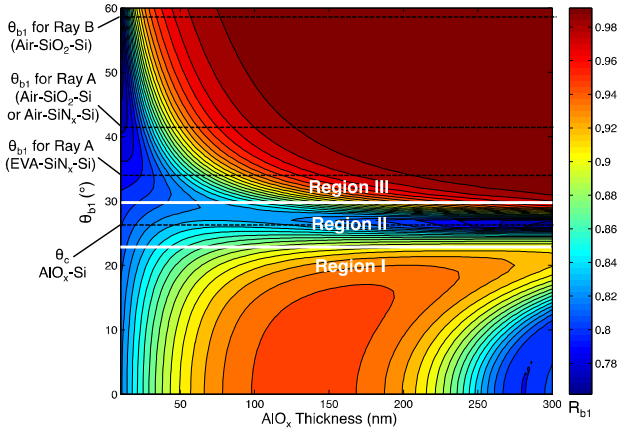

Figure 4: Internal BR contour map for rearside SLDC with AlO_x, highlighting the three regions of interest and θ_{b1} values for primary rays of cells with and without encapsulation.

In this case of a SLDC with AlO_x, the primary rays for cells with and without encapsulation fall within Region III. Therefore, layer thickness isn't very critical, as long as it beyond a certain thickness. Based on cost considerations, the AlO_x film thickness should be limited. As mentioned before for an industrial PERC cell, a lower cost capping layer should be used to prevent the screen printed Al paste from penetrating through the AlO_x. Fig. 5 shows results for a SiN_x capping layer with two different AlO_x thicknesses (20 nm, 75 nm).

In this case, due to the higher index of refraction of SiN_x compared to AlO_x, the poorly reflecting Region II is effectively shifted to higher values of θ_{b1}. While this doesn't significantly affect the unencapsulated cell case, it could reduce the internal BR for encapsulated cells, which have a smaller θ_{b1}.

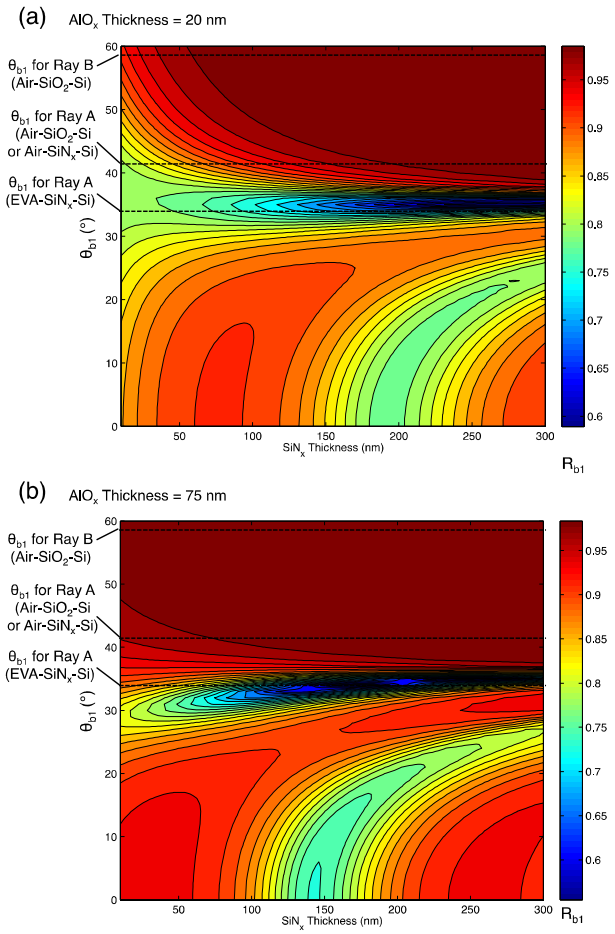

Figure 5: Internal BR contour maps for rearside DLDC with AlO_x-SiN_x as a function of SiN_x thickness and θ_{b1} for two fixed AlO_x thicknesses: (a) 20 nm and (b) 75 nm. The θ_{b1} values for primary rays are also included.

Results for DLDC configurations with TiO_2 and SiO_2 capping layers have also been included (amorphous TiO_2 with a refractive index of 2.0 assumed), both with a fixed AlO_x thickness of 20 nm (Fig. 6). The lower refractive index of SiO_2 ensures that Region II is suppressed to values below that of the θ_{b1} values for the primary rays of interest. The amorphous TiO_2 is found to be almost identical to that of the SiN_x results due to the similar refractive index values.

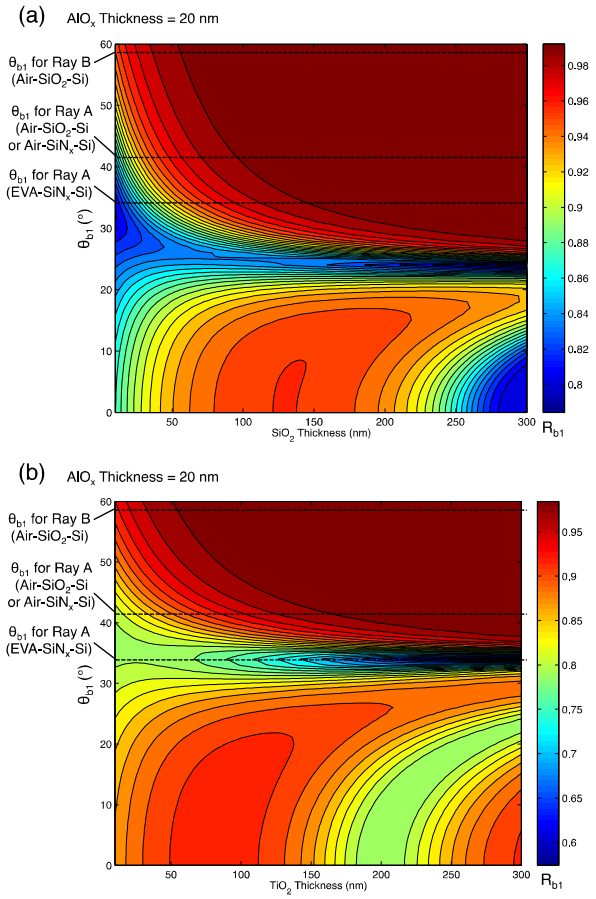

Figure 6: Internal BR contour maps for rearside DLDC with (a) AlO_x-SiO_2 and (b) AlO_x-TiO_2.

CONCLUSION

In conclusion, the internal back reflectance has been modeled as a function of dielectric layer thickness and the backside angle of incidence at the Si-dielectric interface. Single and double layer dielectric rearside coatings have been considered, using AlO_x, SiN_x, TiO_2 and SiO_2. The results clearly show the three critical regions, in terms of backside angle of incidence, for these configurations: $\theta_{b1} < \theta_c$; θ_{b1} near θ_c; and $\theta_{b1} > \theta_c$. For DLDC configurations with a thicker second layer, the second region (near θ_c) is shifted to either higher angles of incidence (for SiN_x and TiO_2) or lower angles (for SiO_2). This affect could play an important role in the internal back reflectance of encapsulated cells with rearside dielectric configurations.

REFERENCES

[1] "U.S. Solar Energy Trade Assessment", GTM 2011.

[2] M. J. McCann, K. R. Catchpole, K. J. Weber, and A. W. Blakers, "A review of thin-film crystalline silicon for solar cell applications. Part 1: Native substrates," *Solar Energy Materials and Solar Cells,* vol. 68, pp. 135-171, 2001.

[3] K. R. Catchpole, M. J. McCann, K. J. Weber, and A. W. Blakers, "A review of thin-film crystalline silicon for solar cell applications. Part 2: Foreign substrates," *Solar Energy Materials and Solar Cells,* vol. 68, pp. 173-215, 2001.

[4] G. P. Willeke, "Thin crystalline silicon solar cells," *Solar Energy Materials and Solar Cells,* vol. 72, pp. 191-200, 2002.

[5] X. F. Brun and S. N. Melkote, "Analysis of stresses and breakage of crystalline silicon wafers during handling and transport," *Solar Energy Materials and Solar Cells,* vol. 93, pp. 1238-1247, 2009.

[6] A. Schneider, C. Gerhards, P. Fath, E. Bucher, R. J. S. Young, J. A. Raby, and A. F. Carroll, "Bow reducing factors for thin screenprinted mc-Si solar cells with Al BSF," in *29th IEEE PVSC*, New Orleans, LA, 2002.

[7] B. Hoex, J. J. H. Gielis, M. C. M. van de Sanden, and W. M. M. Kessels, "On the c-Si surface passivation mechanism by the negative-charge-dielectric Al_2O_3," *Journal of Applied Physics,* vol. 104, p. 113703, 2008.

[8] H. M. Branz, C. W. Teplin, M. J. Romero, I. T. Martin, Q. Wang, K. Alberi, D. L. Young, and P. Stradins, "Hot-wire chemical vapor deposition of epitaxial film crystal silicon for photovoltaics," *Thin Solid Films,* vol. 519, pp. 4545-4550, 2011.

[9] E. D. Palik, *Handbook of Optical Constants of Solids*: Academic Press, 1997.

[10] J. Schmidt, A. Merkle, R. Brendel, B. Hoex, M. C. M. v. de Sanden, and W. M. M. Kessels, "Surface passivation of high-efficiency silicon solar cells by atomic-layer-deposited Al_2O_3," *Progress in Photovoltaics: Research and Applications,* vol. 16, pp. 461-466, 2008.

[11] T. Lauermann, T. Lüder, S. Scholz, B. Raabe, G. Hahn, and B. Terheiden, "Enabling dielectric rear side passivation for industrial mass production by developing lean printing-based solar cell processes," in *35th IEEE PVSC* Honolulu, HI, 2010.

[12] A. Lorenz, J. John, B. Vermang, E. Cornagliotti, and J. Poortmans, "Comparison of illumination level dependency and rear side reflectance of PERC type cells with different dielectric passivation stacks," in *26th EUPVSEC*, Hamburg, Germany, 2011.

[13] D. Kray, M. Hermle, and S. W. Glunz, "Theory and experiments on the back side reflectance of silicon wafer solar cells," *Progress in Photovoltaics: Research and Applications,* vol. 16, pp. 1-15, 2008.

[14] M. A. Green, *Silicon Solar Cells: Advanced Principles & Practice*. Sydney, Austrailia: Centre for Photovoltaic Devices and Systems, University of New South Wales, 1995.

[15] A. Yariv and P. Yeh, *Photonics: Optical Electronics in Modern Communications*, 6th ed: Oxford University Press, 2007.

[16] A. Szeghalmi, M. Helgert, R. Brunner, F. Heyroth, U. Gösele, and M. Knez, "Atomic layer deposition of Al2O3 and TiO2 multilayers for applications as bandpass filters and antireflection coatings," *Applied Optics,* vol. 48, pp. 1727-1732, 2009.

[17] S. C. Baker-Finch and K. R. McIntosh, "Reflection distributions of textured monocrystalline silicon: implications for silicon solar cells," *Progress in Photovoltaics: Research and Applications,* 2012.